

in this previous study. Such effects on the ovarian steroidogenesis may explain why continuous diestrus was observed in the recovery group in this study because estrogen and progesterone, which are steroid hormones synthesized from cholesterol in the ovary, play an important role in controlling the estrous cycle (OECD, 2009). Continuous diestrus indicates at least the temporary and possibly permanent cessation of follicular development and ovulation, and thus temporary infertility (Parker, 2006). In this study, the lack of an effect on the copulation and fertility indices was consistent with the findings that the abnormal estrous cycle was observed after the 27th day of the administration period in the recovery group and not found during the 14-day pre-mating period in the main group. Considering that continuous diestrus was induced around the same time as changes in body weight and food consumption became apparent, the disruption of energy homeostasis could be a factor in the abnormal estrous cycles observed in this study. Food restriction in rats has been shown to result in weight loss and constant diestrus (Kotsuji et al., 1986; Narita et al., 2011). Recent evidence has suggested that many of the central and peripheral endocrine signals that govern energy homeostasis are involved in the control of reproductive function by acting at different levels of the hypothalamic-pituitary-gonadal axis (Narita et al., 2011). Effects on estrous cyclicity have not been reported for the other PFCAs, which may be because the reproductive toxicity of the other PFCAs were not examined at doses causing severe inhibition of body weight gain as observed in the 2.5 mg/kg/day PFDoA group.

PFDoA exerted no effects on the copulation and fertility indices or on the number of corpora lutea and implantation; however, only one of twelve pregnant females delivered live pups in the 2.5 mg/kg/day group. As mentioned above, PFDoA has been reported to disrupt ovarian steroidogenesis (Shi et al., 2009b). Since pregnancy is maintained under the control of estradiol and progesterone (Ogle et al., 1990; Bartholomeusz et al., 1999), PFDoA may affect pregnancy by disrupting steroidogenesis. Another possible factor is impaired fetal development, which could affect the maintenance of pregnancy and normal delivery. Live pups delivered from one pregnant female in the 2.5 mg/kg/day group had markedly lower body weights than those of the controls. The effects of PFDoA on fetal development could be attributed to secondary effects due to maternal toxicity; however, the lipophilic properties of PFDoA (Inoue et al., 2012) also indicate the possibility that it was transferred via the placenta and directly affected the fetuses.

In this study, some of the changes observed during and at the end of the administration period were detected even after the 14-day recovery period, including reductions in body weight, hypertrophy of hepatocytes, bilirubin disposition, peribiliary infiltration of inflammatory cells and bile duct proliferation in the liver, and atrophy of the adrenal cortex. Although no data are currently available on the toxicokinetics of PFDoA, previous studies demonstrated that PFCAs with a

longer carbon chain were eliminated more slowly from the body; the elimination half-life was shown to be 6.38 h for perfluorobutanoic acid (C4), 2.4 h for perfluoroheptanoic acid (C7), 135–185 h for PFOA (C8), 710 hours for PFNA (C9), and 958 h for PFDeA (C10) in male rats intravenously administered PFCAs (Kudo et al., 2002; Kemper, 2003; Ohmori et al., 2003; Chang et al., 2008). Therefore, incomplete recovery of the toxic effects caused by PFDoA may be attributed to its slow elimination from the body.

In summary, 42- to 47-day oral gavage administration of PFDoA mainly affected the liver, causing hypertrophy, necrosis, and inflammatory cholestasis, at 0.5 and 2.5 mg/kg/day. In the 2.5 mg/kg/day group, body weight gain was markedly inhibited, and various changes, mostly viewed as secondary effects, were observed in the bone marrow, spleen, thymus, and adrenal gland. These toxic effects did not recover completely during the 14-day recovery period. Regarding reproductive/developmental toxicity, various histopathological changes, including decreased spermatid and spermatozoa counts, were observed in the male reproductive organs, and continuous diestrus was found in females in the 2.5 mg/kg/day group. Seven of twelve females receiving 2.5 mg/kg/day died during late pregnancy while four other females in this group did not deliver live pups. Based on these findings, the NOAELs of PFDoA were concluded to be 0.1 mg/kg/day for repeated dose toxicity and 0.5 mg/kg/day for the reproductive/developmental toxicity.

## REFERENCES

- Ahrens L, Siebert U, Ebinghaus R. 2009. Temporal trends of polyfluoroalkyl compounds in harbor seals (*Phoca vitulina*) from the German Bight, 1999–2008. *Chemosphere* 76:151–158.
- ATSDR. 2009. Toxicological Profile for Perfluoroalkyls (Draft for Public Comment), US Department of health and human services, Public health service, Agency for Toxic Substances and Disease Registry (ATSDR). Accessed on February 28, 2014.
- Bartholomeusz RK, Bruce NW, Lynch AM. 1999. Embryo survival, and fetal and placental growth following elevation of maternal estradiol blood concentrations in the rat. *Biol Reprod* 61:46–50.
- Biegel LB, Hurtt ME, Frame SR, O'Connor JC, Cook JC. 2001. Mechanisms of extrahepatic tumor induction by peroxisome proliferators in male CD rats. *Toxicol Sci* 60:44–55.
- Biegel LB, Liu RC, Hurtt ME, Cook JC. 1995. Effects of ammonium perfluorooctanoate on Leydig cell function: in vitro, in vivo, and ex vivo studies. *Toxicol Appl Pharmacol* 134:18–25.
- Bookstaff RC, Moore RW, Ingall GB, Peterson RE. 1990. Androgenic deficiency in male rats treated with perfluorodecanoic acid. *Toxicol Appl Pharmacol* 104:322–333.
- Chang SC, Das K, Ehresman DJ, Ellefson ME, Gorman GS, Hart JA, Noker PE, Tan YM, Lieder PH, Lau C, Olsen GW, Butenhoff JL. 2008. Comparative pharmacokinetics of perfluorobutyrates in rats, mice, monkeys, and humans and relevance to human exposure via drinking water. *Toxicol Sci* 104:40–53.

- Clara M, Scheffknecht C, Scharf S, Weiss S, Gans O. 2008. Emissions of perfluorinated alkylated substances (PFAS) from point sources—Identification of relevant branches. *Water Sci Technol* 58:59–66.
- Corton JC, Lapinskas PJ, Gonzalez FJ. 2000. Central role of PPARalpha in the mechanism of action of hepatocarcinogenic peroxisome proliferators. *Mutat Res* 448:139–151.
- Ding L, Hao F, Shi Z, Wang Y, Zhang H, Tang H, Dai J. 2009. Systems biological responses to chronic perfluorododecanoic acid exposure by integrated metabolomic and transcriptomic studies. *J Proteome Res* 8:2882–2891.
- Falandysz J, Taniyasu S, Gulkowska A, Yamashita N, Schulte-Oehlmann U. 2006. Is fish a major source of fluorinated surfactants and repellents in humans living on the Baltic Coast? *Environ Sci Technol* 40:748–751.
- Feng Y, Fang X, Shi Z, Xu M, Dai J. 2010. Effects of PFNA exposure on expression of junction-associated molecules and secretory function in rat Sertoli cells. *Reprod Toxicol* 30:429–437.
- Feng Y, Shi Z, Fang X, Xu M, Dai J. 2009. Perfluorononanoic acid induces apoptosis involving the Fas death receptor signaling pathway in rat testis. *Toxicol Lett* 190:224–230.
- Fujii Y, Yan J, Harada KH, Hitomi T, Yang H, Wang P, Koizumi A. 2012. Levels and profiles of long-chain perfluorinated carboxylic acids in human breast milk and infant formulas in East Asia. *Chemosphere* 86:315–321.
- Green S. 1995. PPAR: a mediator of peroxisome proliferator action. *Mutat Res* 333:101–109.
- Griffith FD, Long JE. 1980. Animal toxicity studies with ammonium perfluorooctanoate. *Am Ind Hyg Assoc J* 41:576–583.
- Guruge KS, Taniyasu S, Yamashita N, Wijeratna S, Mohotti KM, Seneviratne HR, Kannan K, Yamanaka N, Miyazaki S. 2005. Perfluorinated organic compounds in human blood serum and seminal plasma: A study of urban and rural tea worker populations in Sri Lanka. *J Environ Monit* 7:371–377.
- Hamid J, Sayeed A, McFarlane H. 1974. The effect of 1-(o-chlorophenyl)-1-(p-chlorophenyl)-2,2-dichloroethane(o,p'-DDD) on the immune response in malnutrition. *Br J Exp Pathol* 55:94–100.
- Harada KH, Hitomi T, Niisoe T, Takanaka K, Kamiyama S, Watanabe T, Moon CS, Yang HR, Hung NN, Koizumi A. 2011. Odd-numbered perfluorocarboxylates predominate over perfluorooctanoic acid in serum samples from Japan, Korea and Vietnam. *Environ Int* 37:1183–1189.
- Haug LS, Huber S, Schlabach M, Becher G, Thomsen C. 2011. Investigation on per- and polyfluorinated compounds in paired samples of house dust and indoor air from Norwegian homes. *Environ Sci Technol* 45:7991–7998.
- Haug LS, Thomsen C, Becher G. 2009. Time trends and the influence of age and gender on serum concentrations of perfluorinated compounds in archived human samples. *Environ Sci Technol* 43:2131–2136.
- Hirata-Koizumi M, Fujii S, Furukawa M, Ono A, Hirose A. 2012. Repeated dose and reproductive/developmental toxicity of perfluorooctadecanoic acid in rats. *J Toxicol Sci* 37:63–79.
- Hoff PT, Scheirs J, Van de Vijver K, Van Dongen W, Esmans EL, Blust R, De Coen W. 2004. Biochemical effect evaluation of perfluorooctane sulfonic acid-contaminated wood mice (*Apodemus sylvaticus*). *Environ Health Perspect* 112:681–686.
- Holden PR, Tugwood JD. 1999. Peroxisome proliferator-activated receptor alpha: Role in rodent liver cancer and species differences. *J Mol Endocrinol* 22:1–8.
- Inoue Y, Hashizume N, Yakata N, Murakami H, Suzuki Y, Kikushima E, Otsuka M. 2012. Unique physicochemical properties of perfluorinated compounds and their bioconcentration in common Carp *Cyprinus carpio* L. *Arch Environ Contam Toxicol* 62:672–680.
- JALAS. 1987. Guidelines for Animal Experimentation, Japanese Association for Laboratory Animal Science, dated May 22, 1987.
- Japanese Animal Welfare Law. 2006. Act on Welfare and Management of Animals. Act No. 105 of October 1, 1973. As amended up to Act No. 50 of June 2, 2006.
- Jensen AA, Leffers H. 2008. Emerging endocrine disruptors: Perfluoroalkylated substances. *Int J Androl* 31:161–169.
- Kemper RA. 2003. Perfluorooctanoic acid: Toxicokinetics in the rat. Association of Plastics Manufactures of Europe. Submitted to the US EPA's Administrative Record. AR226–1499, cited in ASTDR (2009).
- Kotsuji F, Goto K, Aso T, Tominaga T. 1986. The influence of weight loss on the reproductive function of the female rat: Changes in the estrous cycle and hypothalamo-pituitary-ovarian function during feed restriction and subsequent refeeding period (in Japanese). *Nihon Sanka Fujinka Gakkai Zasshi* 38:1713–1721.
- Kudo N, Katakura M, Sato Y, Kawashima Y. 2002. Sex hormone-regulated renal transport of perfluorooctanoic acid. *Chem Biol Interact* 139:301–316.
- Kudo N, Suzuki-Nakajima E, Mitsumoto A, Kawashima Y. 2006. Responses of the liver to perfluorinated fatty acids with different carbon chain length in male and female mice: In relation to induction of hepatomegaly, peroxisomal beta-oxidation and microsomal 1-acylglycerophosphocholine acyltransferase. *Biol Pharm Bull* 29:1952–1957.
- Kunacheva C, Tanaka S, Fujii S, Boontanon SK, Musirat C, Wongwattana T, Shivakoti BR. 2011. Mass flows of perfluorinated compounds (PFCs) in central wastewater treatment plants of industrial zones in Thailand. *Chemosphere* 83:737–744.
- Lau C, Anitole K, Hodes C, Lai D, Pfahles-Hutchens A, Seed J. 2007. Perfluoroalkyl acids: A review of monitoring and toxicological findings. *Toxicol Sci* 99:366–394.
- Li Y, Ramdhan DH, Naito H, Yamagishi N, Ito Y, Hayashi Y, Yanagiba Y, Okamura A, Tamada H, Gonzalez FJ, Nakajima T. 2011. Ammonium perfluorooctanoate may cause testosterone reduction by adversely affecting testis in relation to PPARalpha. *Toxicol Lett* 205:265–272.
- Martin JW, Mabury SA, Solomon KR, Muir DC. 2003. Bioconcentration and tissue distribution of perfluorinated acids in rainbow trout (*Oncorhynchus mykiss*). *Environ Toxicol Chem* 22:196–204.

- MOE. 2006. Standards Relating to the Care, Management of Laboratory Animals and Relief of Pain. Announcement No. 88 of Ministry of the Environment (MOE), Japan, dated April 28, 2006.
- MOE, METI, MHLW. 2008. Standard concerning testing laboratories implementing tests for new chemical substances etc. Joint notification by director generals of Environmental Policy Bureau, Ministry of the Environment (MOE), Japan (Kanpokihatsu No. 031121004) and Manufacturing Industries Bureau, Ministry of Economy, Trade and Industry (METI), Japan (Seikyokuhatsu No. 3), dated November 17, 2003 and by director general of Pharmaceutical and Food Safety Bureau, Ministry of Health, Labour and Welfare (MHLW), Japan (Yakusyokuhatsu No. 1121003), dated November 21, 2003. As amended up to July 4, 2008.
- Moriyama T, Tsujioka S, Ohira T, Nonaka S, Ikeda H, Sugiura H, Tomohiro M, Samura K, Nishikibe M. 2008. Effects of reduced food intake on toxicity study parameters in rats. *J Toxicol Sci* 33:537–547.
- Murakami M, Shinohara H, Takada H. 2009. Evaluation of wastewater and street runoff as sources of perfluorinated surfactants (PFSs). *Chemosphere* 74:487–493.
- Narita K, Nagao K, Bannai M, Ichimaru T, Nakano S, Murata T, Higuchi T, Takahashi M. 2011. Dietary deficiency of essential amino acids rapidly induces cessation of the rat estrous cycle. *PLoS One* 6:e28136.
- Nishikoori H, Murakami M, Sakai H, Oguma K, Takada H, Takizawa S. 2011. Estimation of contribution from non-point sources to perfluorinated surfactants in a river by using boron as a wastewater tracer. *Chemosphere* 84:1125–1132.
- O'Connor JC, Frame SR, Ladies GS. 2002. Evaluation of a 15-day screening assay using intact male rats for identifying steroid biosynthesis inhibitors and thyroid modulators. *Toxicol Sci* 69:79–91.
- OECD. 1996. Organisation for Economic Co-operation and Development (OECD) Guidelines for the Testing of Chemicals, Section 4: Health Effects, Test No. 422: Combined Repeated Dose Toxicity Study with the Reproduction/Developmental Toxicity Screening Test. Adopted on 22 March, 1996.
- OECD. 2009. Guidance Document for Histologic Evaluation of Endocrine and Reproductive Tests in Rodents Series on testing and assessment, number 106. OECD, Environmenta directorate, Joint meeting of the chemicals committee and the working party on chemicals, pesticides and iotechnology, Available at: [http://www.oecd.org/officialdocuments/displaydocumentpdf/?cote=env/jm/mono\(2009\)11&doclanguage=en](http://www.oecd.org/officialdocuments/displaydocumentpdf/?cote=env/jm/mono(2009)11&doclanguage=en), accessed on July 28, 2011.
- Ogle TF, Mills TM, Costoff A. 1990. Progesterone maintenance of the placental progesterone receptor and placental growth in ovariectomized rats. *Biol Reprod* 43:276–284.
- Ohmori K, Kudo N, Katayama K, Kawashima Y. 2003. Comparison of the toxicokinetics between perfluorocarboxylic acids with different carbon chain length. *Toxicology* 184:135–140.
- Olsen GW, Lange CC, Ellefson ME, Mair DC, Church TR, Goldberg CL, Herron RM, Medhdizadehkashi Z, Noblietti JB, Rios JA, Reagan WK, Zobel LR. 2012. Temporal trends of perfluoroalkyl concentrations in American Red Cross Adult Blood Donors, 2000–2010. *Environ Sci Technol* 46:6330–6338.
- Parker RM. 2006. Testing for reproductive toxicity. In: Hood RD, editor. *Developmental and Reproductive Toxicology—A Practical Approach*. Florida: CRC Press, Taylor & Fransis Group. pp 425–487.
- Perkins RG, Butenhoff JL, Kennedy GL Jr, Palazzolo MJ. 2004. 13-week dietary toxicity study of ammonium perfluorooctanoate (APFO) in male rats. *Drug Chem Toxicol* 27: 361–378.
- Permadi H, Lundgren B, Andersson K, Sundberg C, DePierre JW. 1993. Effects of perfluoro fatty acids on peroxisome proliferation and mitochondrial size in mouse liver: dose and time factors and effect of chain length. *Xenobiotica* 23:761–770.
- Prevedouros K, Cousins IT, Buck RC, Korzeniowski SH. 2006. Sources, fate and transport of perfluorocarboxylates. *Environ Sci Technol* 40:32–44.
- Rosol TJ, Yarrington JT, Latendresse J, Capen CC. 2001. Adrenal gland: structure, function, and mechanisms of toxicity. *Toxicol Pathol* 29:41–48.
- Shallie PD, Fakoya FA, Fakunle PB, Haruna MT, Shotunde DF. 2012. Dietary stress and energy metabolism: Evaluation of the adrenal cortex. *Webmed Central BIOCHEMISTRY* 3: WMC003472.
- Shi Z, Ding L, Zhang H, Feng Y, Xu M, Dai J. 2009a. Chronic exposure to perfluorododecanoic acid disrupts testicular steroidogenesis and the expression of related genes in male rats. *Toxicol Lett* 188:192–200.
- Shi Z, Feng Y, Wang J, Zhang H, Ding L, Dai J. 2010a. Perfluorododecanoic acid-induced steroidogenic inhibition is associated with steroidogenic acute regulatory protein and reactive oxygen species in cAMP-stimulated Leydig cells. *Toxicol Sci* 114:285–294.
- Shi Z, Zhang H, Ding L, Feng Y, Wang J, Dai J. 2010b. Proteomic analysis for testis of rats chronically exposed to perfluorododecanoic acid. *Toxicol Lett* 192:179–188.
- Shi Z, Zhang H, Ding L, Feng Y, Xu M, Dai J. 2009b. The effect of perfluorododecanonic acid on endocrine status, sex hormones and expression of steroidogenic genes in pubertal female rats. *Reprod Toxicol* 27:352–359.
- Shi Z, Zhang H, Liu Y, Xu M, Dai J. 2007. Alterations in gene expression and testosterone synthesis in the testes of male rats exposed to perfluorododecanoic acid. *Toxicol Sci* 98:206–215.
- Tao L, Kannan K, Kajiwara N, Costa MM, Fillmann G, Takahashi S, Tanabe S. 2006. Perfluorooctanesulfonate and related fluorochemicals in albatrosses, elephant seals, penguins, and polar skuas from the Southern Ocean. *Environ Sci Technol* 40:7642–7648.
- Thompson J, Roach A, Eaglesham G, Bartkow ME, Edge K, Mueller JF. 2011. Perfluorinated alkyl acids in water, sediment and wildlife from Sydney Harbour and surroundings. *Mar Pollut Bull* 62:2869–2875.
- UK COT. 2006. COT statement on the tolerable risk daily intake for perfluorooctanoic acid, Committee on toxicity of chemicals on food, consumer products and the environment, October 2006.

- US EPA. 2013. Perfluorooctanoic acid (PFOA) and fluorinated telomers, last updated on November 4, 2013. United States Environmental Protection Agency (US EPA). Available at: <http://www.epa.gov/oppt/pfoa/>. Accessed on February 28, 2014.
- Van de Vijver KI, Holsbeek L, Das K, Blust R, Joiris C, De Coen W. 2007. Occurrence of perfluorooctane sulfonate and other perfluorinated alkylated substances in harbor porpoises from the Black Sea. *Environ Sci Technol* 41: 315–320.
- Wang T, Lu Y, Chen C, Naile JE, Khim JS, Giesy JP. 2012. Perfluorinated compounds in a coastal industrial area of Tianjin, China. *Environ Geochem Health* 34:301–311.
- Wolf CJ, Schmid JE, Lau C, Abbott BD. 2012. Activation of mouse and human peroxisome proliferator-activated receptor-alpha (PPARalpha) by perfluoroalkyl acids (PFAAs): Further investigation of C4-C12 compounds. *Reprod Toxicol* 33:546–551.
- Yang Q, Xie Y, Alexson SE, Nelson BD, DePierre JW. 2002. Involvement of the peroxisome proliferator-activated receptor alpha in the immunomodulation caused by peroxisome proliferators in mice. *Biochem Pharmacol* 63:1893–1900.
- Zhang H, Shi Z, Liu Y, Wei Y, Dai J. 2008. Lipid homeostasis and oxidative stress in the liver of male rats exposed to perfluorododecanoic acid. *Toxicol Appl Pharmacol* 227: 16–25.

## Isotope Microscopy Visualization of the Adsorption Profile of 2-Methylisoborneol and Geosmin in Powdered Activated Carbon


Yoshihiko Matsui,<sup>\*,†</sup> Asuka Sakamoto,<sup>‡</sup> Soichi Nakao,<sup>‡</sup> Takuma Taniguchi,<sup>‡</sup> Taku Matsushita,<sup>†</sup> Nobutaka Shirasaki,<sup>†</sup> Naoya Sakamoto,<sup>§</sup> and Hisayoshi Yurimoto<sup>§,||</sup>

<sup>†</sup>Faculty of Engineering, Hokkaido University, N13W8, Sapporo 060-8628, Japan

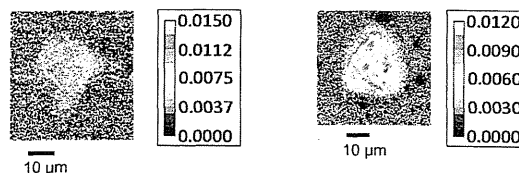
<sup>‡</sup>Graduate School of Engineering, Hokkaido University, N13W8, Sapporo 060-8628, Japan

<sup>§</sup>Isotope Imaging Laboratory, Creative Research Institution, Hokkaido University, N21W10, Sapporo, 001-0021, Japan

<sup>||</sup>Natural History Sciences, Hokkaido University, N10W8, Sapporo 060-0810, Japan

 Supporting Information

**ABSTRACT:** Decreasing the particle size of powdered activated carbon may enhance its equilibrium adsorption capacity for small molecules and micropollutants, such as 2-methylisoborneol (MIB) and geosmin, as well as for macromolecules and natural organic matter. Shell adsorption, in which adsorbates do not completely penetrate the adsorbent but instead preferentially adsorb near the outer surface of the adsorbent, may explain this enhancement in equilibrium adsorption capacity. Here, we used isotope microscopy and deuterium-doped MIB and geosmin to directly visualize the solid-phase adsorbate concentration profiles of MIB and geosmin in carbon particles. The deuterium/hydrogen ratio, which we used as an index of the solid-phase concentration of MIB and geosmin, was higher in the shell region than in the inner region of carbon particles. Solid-phase concentrations of MIB and geosmin obtained from the deuterium/hydrogen ratio roughly agreed with those predicted by shell adsorption model analyses of isotherm data. The direct visualization of the localization of micropollutant adsorbates in activated carbon particles provided direct evidence of shell adsorption.



### 1. INTRODUCTION

Adsorption by powdered activated carbon (PAC) is a widely used method for removing micropollutants, in particular hydrophobic compounds, such as 2-methylisoborneol (MIB) and geosmin, earthy musty-smelling substances, in water treatment plants.<sup>1,2</sup> Although the MIB and geosmin adsorption capacities on PAC are high, the capacities are not fully utilized if the PAC–water contact times are insufficient, because adsorption kinetics are slow. To overcome the slow adsorption kinetics, superfine powdered activated carbon (SPAC) of particle diameter <1 μm is produced by microgrinding.<sup>3</sup> SPAC has also attracted attention, in particular for its potential use in combination with membrane microfiltration techniques.<sup>4–7</sup> In addition to SPAC having much faster adsorption kinetics than conventionally sized PAC, recent research has shown that SPAC has a greater equilibrium capacity to adsorb certain compounds such as large, chromophoric constituents of organic matter.<sup>3,8</sup> This increase in equilibrium adsorption capacity was not predicted because PAC and SPAC that was produced by microgrinding the PAC had a similar internal pore volume and a similar internal surface area. It has been traditionally thought that changing the particle size will not change its equilibrium adsorption capacity and the adsorption capacity of activated carbon does not depend on particle size because adsorption occurs in internal pores of activated carbon particles.<sup>9</sup>

In porous adsorbents, the increase in equilibrium adsorption capacity with decreasing particle size can be explained by shell adsorption, where adsorbates do not completely penetrate the adsorbent particle but instead preferentially adsorb near the outer surface of the particle (Supporting Information (SI) Figure S1).<sup>10</sup> Ando et al.<sup>11</sup> confirm the occurrence of shell adsorption for the adsorption of polystyrenesulfonate (molecular weight, 6000 Da) on carbon particles by directly observing intraparticle solid-phase concentration profiles of polystyrenesulfonate. As an index of polystyrenesulfonate concentration, they measured the emission of X-rays from sulfur atoms present in the polystyrenesulfonate by means of field emission–scanning electron microscopy/energy-dispersive X-ray spectrometry (FE-SEM/EDXS).

Our research group recently determined that the single-solute equilibrium capacity of activated carbon to adsorb MIB and geosmin, which are both small, nonchromophoric molecules, may be particle size–dependent. The occurrence of shell adsorption may accurately explain this phenomenon, but no direct evidence to support this hypothesis exists to date. Direct evidence is obtainable by observing the intraparticle concentration profile of MIB and geosmin. However, applicable

Received: May 20, 2014

Revised: August 25, 2014

Accepted: August 27, 2014

Published: August 27, 2014

Table 1. Characteristics of the Activated Carbons Examined<sup>a</sup>

	median diameter ( $D_{50}$ , $\mu\text{m}$ )		raw material	origin of conventionally sized PAC	isotherm	$\alpha$ (SAM parameter) $\mu\text{m}^{-1}$
	conventionally sized PAC	superfine PAC				
carbon-A	31	2.6, 0.72, 0.50	coconut shell	SP23, Pica	MIB Geosmin	0.24 0.32
carbon-B	25	3.1, 0.85, 0.52	wood	MP23, Pica	MIB Geosmin	0.03 0.20
carbon-C	19	4.9, 0.62	wood	Taiko W, Futamura Chemical Co., Ltd.	MIB	0.09

<sup>a</sup>MIB, 2-methylisoborneol; PAC, powdered activated carbon; SAM, shell adsorption model.

methods have been limited. Very sophisticated methods such as measurements by means of atomic force microscopy can be applicable for the observation and determination of adsorption on flat model surfaces, but not for so well-defined and complicated surfaces such as activated carbon and cotton surfaces because of their shape, porous structure, and structural heterogeneity.<sup>12–14</sup> Fluorescence spectroscopy of the cotton surface that adsorbed fluorescently labeled polymer could determine the extent of adsorption,<sup>15,16</sup> but the method is not applicable for observing intraparticle concentration profile. Microprobe laser-desorption laser-ionization mass spectroscopy is used to spatially resolve intraparticle concentration profiles within several granular adsorbents,<sup>17</sup> but it is not applicable to resolve profiles within adsorbents of particle diameter <30  $\mu\text{m}$ . Direct observation with FE-SEM/EDXS has higher resolution but is not applicable for examining the adsorption of MIB and geosmin because these molecules do not contain a suitable marker atom since their constituent atoms are the same as those of activated carbon. These two methods give one-dimensional intraparticle concentration profile, but they cannot visualize concentration profile as a two-dimensional map.

Secondary ion mass spectrometry has been used to identify microscale isotope ratios in cosmic particles.<sup>18</sup> Isotope microscope systems, which are secondary ion mass spectrometers coupled with solid-state imaging detectors, enable microimaging of two-dimensional isotope ratios (e.g., deuterium/hydrogen ratio,  $^2\text{D}/^1\text{H}$ ) with permil-level precision and high mass resolution.<sup>19–21</sup> Recently, isotope microscope systems have been used to analyze living matter and semiconductor specimens, in particular, isotope-doped samples.<sup>22</sup>

The objective of the present study was to visualize, for the first time, the intraparticle adsorption profile of trace organic compounds in PAC particles. The two taste and odor compounds, MIB and geosmin, were used as probe compounds in deuterium-labeled form. MIB and geosmin concentration profiles were visualized by using isotope microscopy to determine whether the phenomenon of the shell adsorption can explain the particle-size dependence of the equilibrium adsorption capacity of small, nonchromophoric adsorbates.

## 2. MATERIALS AND METHODS

**2.1. Activated Carbons.** Commercially available PACs of conventional particle size (median diameter >10  $\mu\text{m}$ , Table 1) were obtained and prepared as slurries in ultrapure water (5% by weight). The PACs were pulverized into SPAC by wet grinding with a bead mill (Metawater Co., Tokyo, Japan). Median diameter SPAC particles ranged from 0.5 to 4.9  $\mu\text{m}$  (Table 1, SI Figure S2). In the text, we refer to these activated carbons by using parenthetic numbers to indicate the particle median diameter in micrometers, for example, Carbon-A (31)

represents the as-received form of Carbon-A. The activated carbons were stored as slurries in ultrapure water (Milli-Q Advantage, Millipore Co.) at 4 °C. Prior to use in experiments, slurries were diluted and placed under a vacuum prior to use.

Particle size distributions of the activated carbons were determined with a laser-light scattering particle size analyzer (Microtrac MT3300EXII; Nikkiso Co., Ltd., Tokyo, Japan) following the addition of a dispersant (Triton X-100; Kanto Chemical Co., Inc., Tokyo, Japan; final concentration after addition, 0.08%) and ultrasonic dispersion. Hydrogen contents in ~30-mg samples of each carbon were determined with an elemental analyzer (CHNS mode, 1150 °C in combustion tubes, 850 °C in reduction tube, vario EL cube, Elementar Analysensysteme GmbH, Germany). Prior to H analysis, carbons were dried for 12 hours at a temperature of 105 °C and cooled in a desiccator.

**2.2. Adsorbates and Water Samples.** Stock solutions of MIB and geosmin were prepared by dissolving pure MIB or geosmin (Wako Pure Chemical Industries, Ltd., Osaka, Japan) in ultrapure water and then filtering the water through a 0.2  $\mu\text{m}$  pore size membrane filter (DISMIC-25HP; Toyo Roshi Kaisha, Ltd., Tokyo). Organic-free water was prepared by amending ultrapure water with inorganic ions such that conductivity was 77–89  $\mu\text{S}/\text{cm}$  and the ionic composition was similar to that used in a previous study.<sup>3,23</sup> However, natural organic matter, which largely affects the adsorption of MIB and geosmin on activated carbon, was not added. The organic-free water was spiked with the MIB or geosmin stock solutions to prepare samples with an initial MIB or geosmin concentration of ~1  $\mu\text{g}/\text{L}$ , since MIB and geosmin occur naturally at concentrations usually lower than 1  $\mu\text{g}/\text{L}$ . The water samples were adjusted to pH 7.0  $\pm$  0.1 with HCl or NaOH as required. The concentrations of MIB and geosmin were confirmed by using a purge and trap concentrator (Aqua PT 5000 J; GL Sciences, Inc., Tokyo, Japan) coupled to a gas chromatograph–mass spectrometer (GCMS-QP2010 Plus; Shimadzu Corp., Kyoto, Japan).

**2.3. Batch Adsorption Equilibrium Tests.** Aliquots (150 mL) of the water samples containing MIB or geosmin ( $C_0$  ~1  $\mu\text{g}/\text{L}$ ) were transferred to 160 mL vials. Specified amounts of SPAC or PAC were immediately added (0.05–1.0 mg/L) and the vials manually shaken and then agitated on a mechanical shaker for 1 week at a constant temperature of 20 °C. Preliminary experiments confirmed that the adsorption equilibrium for both MIB and geosmin was reached after 1 week of contact. Control tests were also conducted by using vials that did not contain carbon to confirm that changes in MIB and geosmin concentration during long-term mixing were negligible. After filtering the water samples through a 0.2  $\mu\text{m}$  pore size membrane filter, MIB and geosmin concentrations in the aqueous phase were measured. Solid-phase concentrations

of MIB and geosmin were then calculated from the mass balance.

**2.4. Isotope Microscopy.** To prepare carbon particles loaded with deuterium-doped MIB or geosmin, we conducted batch adsorption experiments in 5 L bottles. Sample solutions containing approximately 1  $\mu\text{g/L}$  deuterium-doped MIB or geosmin (Figure 1) were shaken after the addition of a specified

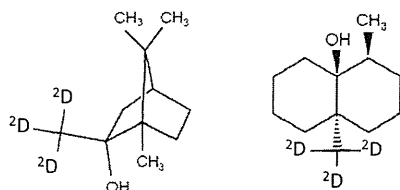


Figure 1. Chemical structures of deuterium-doped 2-methylisoborneol (left) and geosmin (right).

amount of carbon. After the bottles were shaken for 1 week, the carbon particles were recovered. Only the conventionally sized PACs were used for isotope microscopy because the intraparticle solid-phase concentration changed on a micrometer scale; therefore the solid-phase concentration would not measurably change in a SPAC particle. Another reason is that the image resolution of the isotope microscopy method is not sufficient to visualize MIB and geosmin concentration profiles in SPAC particles.

To prepare samples for imaging, the wet carbon particles were placed on an indium plate supported by a silicon wafer and partially embedded into the indium plate manually using gentle pressure. Further sample preparation, such as slicing with a microtome, was not conducted because activated carbon particles are very fragile and the inside of the particle was expected to be exposed during the isotope analysis.

Deuterium/hydrogen isotope analysis of the carbon particles was conducted by using an isotope microscope system (Hokkaido University, Sapporo, Japan) that consisted of a stigmatic secondary ion mass spectrometer (Cameca ims-1270) and a SCAPS (stacked complementary metal-oxide-semiconductor active pixel sensor) ion detector.<sup>19</sup> A 20 keV  $\text{Cs}^+$  primary ion beam was homogeneously irradiated over a  $250 \times 250 \mu\text{m}^2$  sample area to achieve uniform secondary ion-beam emission from an imaging area of  $180 \times 180 \mu\text{m}^2$ . The primary current was adjusted to 60 nA. We supposed that, during the exposure to the irradiation of the primary ion beam, shrinking of the carbon particles in size occurred, as depicted in Figure 2. In particular, the upsides of the carbon particles were removed and the insides of the particles were exposed. The secondary ions were accelerated to 10 keV and captured as mass-filtered ion images projected by the stigmatic ion optics of the secondary ion mass spectrometer. A  $150 \mu\text{m}$  diameter focal plane aperture was used. The SCAPS ion detector was positioned on the projection plane of the mass-filtered secondary ion image. Secondary ion images of  $^1\text{H}^+$  and  $^2\text{D}^+$  were captured by the SCAPS ion detector with a repeated sequence of 5-s ( $^1\text{H}$ ) and 250-s ( $^2\text{D}$ ) detection times. Isotopic maps were obtained by calculating and plotting the  $^2\text{D}/^1\text{H}$  molar ratio for each pixel. Loading of deuterium-doped MIB or geosmin in the carbon particles was expected to yield the  $^2\text{D}/^1\text{H}$  ratio much higher than that of the earth's natural  $^2\text{D}/^1\text{H}$  molar ratio of 0.00015.<sup>24</sup>

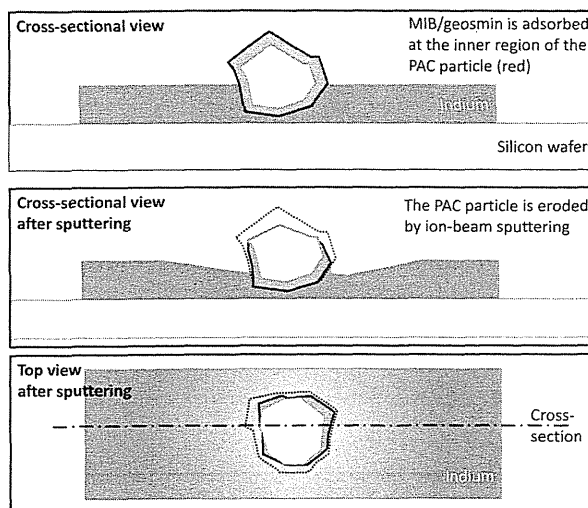


Figure 2. Schematic of the change in particle size caused by ion-beam sputtering in the repeated detection of secondary ions. MIB: 2-methylisoborneol; PAC, powdered activated carbon.

### 3. RESULTS AND DISCUSSION

#### 3.1. Effect of Particle Size on MIB and Geosmin Adsorption Capacity.

The adsorption of MIB on Carbon-A was particle-size dependent (i.e., the equilibrium adsorption capacity was greater for the SPACs than for the PAC). To be precise, the adsorption capacity increased when the particle diameter was decreased from 31 to 2.6  $\mu\text{m}$ , but it did not change when the particle diameter was reduced further, to 0.72 or 0.50  $\mu\text{m}$ . On the other hand, results for Carbon-B and Carbon-C showed only a small particle-size dependency for the entire particle size range tested (25–0.52  $\mu\text{m}$ , Figure 3 and SI Table S1). The adsorption of geosmin on both tested carbons tested (Carbon-A and Carbon-B) was also particle-size dependent, with greater equilibrium adsorption capacity for SPAC than for PAC.

We previously reported that for NOM adsorption, the particle-size dependency of the equilibrium adsorption capacity was not due to the pore size distributions of SPAC and PAC. In this study, we confirmed that the pore size distributions in both mesopore and micropore regions did not change substantially as a result of the pulverization of PAC for the production of SPAC (SI Table S1 and Figure S3). Similarly, changes in BET surface area were small. Therefore, the particle-size dependency of MIB and geosmin adsorption capacities was not related to the pore sizes of the PACs and the SPACs. The particle size dependency was greater for Carbon-A than for Carbon-B and Carbon-C. However, the difference in particle size dependency was also not related to the pore size distributions of the carbons (SI Table S1 and Figure S2). Further research is needed to reach any conclusive remarks regarding the manner in which these characteristics influence the dependency of adsorption capacity on particle size.

Overall, the dependency of the adsorption capacity on particle size was greater for geosmin than for MIB, and geosmin was adsorbed to a greater extent than MIB in both the SPAC and PAC. The effect of adsorbate characteristics on the particle size dependency of the adsorption capacity requires further study. The dependency decreases with the order geosmin > MIB > phenol,<sup>3</sup> where no measurable dependency was

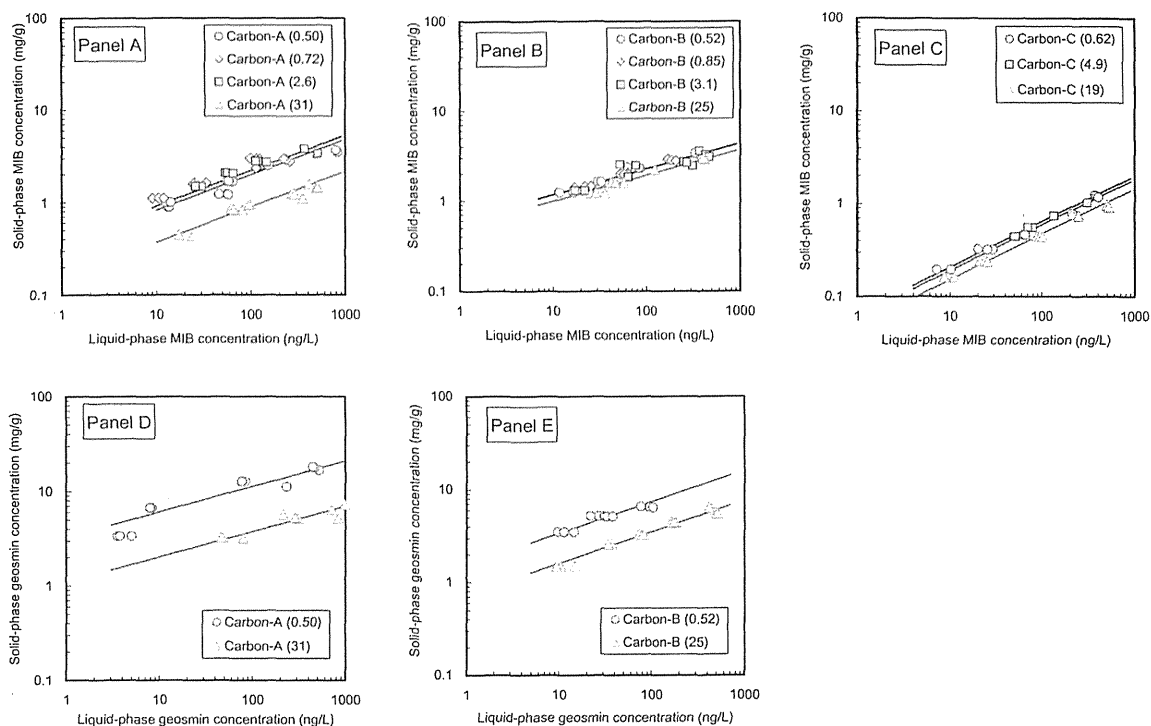


**Figure 3.** Adsorption isotherms of 2-methylisoborneol (MIB; panels A–C) and geosmin (panels D–E). Lines represent fits for the shell adsorption model.

observed for the latter adsorbate.<sup>3</sup> It is possible that the hydrophobicity of the adsorbate plays a role, whose greater particle size dependency is associated with increasing adsorbate hydrophobicity.

**3.2. Prediction of the Solid-Phase Concentration Profiles.** For NOM adsorption, Ando et al.<sup>3</sup> report that the increase in adsorption capacity with decreasing adsorbent particle size is attributable to molecules adsorbing principally in the exterior region close to the external particle surface. The specific external surface area (surface area per unit mass) available for adsorption is greater for smaller adsorbent particles, and hence adsorption capacity is larger on SPAC. The shell adsorption model (SAM) was proposed to describe quantitatively the increase in NOM adsorption capacity with decreasing carbon particle size.<sup>10</sup> In this study, the SAM was applied for MIB and geosmin, and solid-phase concentration profiles in carbon particles were predicted. The SAM utilizes an expanded expression of the Freundlich equation.

$$q_E = KC_E^{1/n} \tag{1}$$

where  $q_E$  is the equilibrium solid-phase concentration of the adsorbate (mg/g),  $C_E$  is the equilibrium aqueous-phase concentration (ng/L),  $K$  is the Freundlich adsorption capacity parameter (mg/g)/(ng/L)<sup>1/n</sup>, and  $n$  is the Freundlich exponent.

In the SAM, the adsorption capacity is locally different in a adsorbent particle, and the local adsorption capacity parameter, that is, the Freundlich  $K_S$  value, decreases linearly with distance from the external surface to a certain depth. When assuming a spherical adsorbent particle:

$$K_S(r, R) = K_0 \times \max[(r - R) \times \alpha + 1, 0] \tag{2}$$

where  $K_S(r, R)$  is the radially changing local Freundlich adsorption capacity parameter (mg/g)/(ng/L)<sup>1/n</sup>,  $r$  is the radial distance from the center of a adsorbent particle ( $\mu\text{m}$ ),  $R$  is the adsorbent particle radius ( $\mu\text{m}$ ),  $K_0$  is the Freundlich parameter of adsorption at the external particle surface (i.e., at  $r = R$ , [mg/g]/[ng/L]<sup>1/n</sup>) and  $\alpha$  is the reciprocal of penetration depth (or thickness of the penetration shell) with the unit  $\mu\text{m}^{-1}$ .

Therefore, the local solid-phase concentration,  $q(r, R)$ , at radial distance  $r$  in an adsorbent with radius  $R$  is given by substituting eq 2 into Freundlich equation.

$$q(r, R) = C_E^{1/n} K_0 \times \max[(r - R) \times \alpha + 1, 0] \tag{3}$$

where  $q(r, R)$  is the radially changing local solid-phase concentration as a function of radial distance  $r$  and carbon particle radius  $R$  (mg/g)/(ng/L)<sup>1/n</sup>.

When the adsorbent particle size is not uniform, the overall adsorption capacity is given by

$$q_E = \int_0^\infty \left\{ \int_0^R r^2 q(r, R) dr \right\} \frac{3f_R(R)}{R^3} dR \tag{4}$$

where  $f_R(R)$  is the normalized particle size distribution function of adsorbent ( $\mu\text{m}^{-1}$ ).

After substituting eq 3 into 4, the isotherm equation of the SAM becomes

$$q_E = C_E^{1/n} K_0 \int_0^\infty \left\{ \int_0^R r^2 \max[(r - R) \times \alpha + 1, 0] dr \right\} \frac{3f_R(R)}{R^3} dR \tag{5}$$

To fit eq 5 to the isotherm data shown in Figure 3, we searched for sets of isotherm parameter values for  $K_0$ ,  $\alpha$ , and  $n$



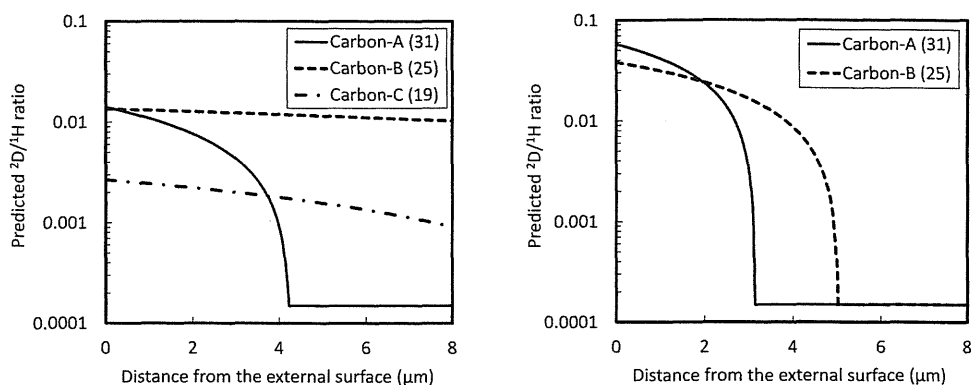


Figure 4. Deuterium/hydrogen ratios against distance from the external surface of a carbon particle predicted by using the shell adsorption model (left, MIB; right, geosmin). Calculations were made for an equilibrium aqueous-phase concentration of 100 ng/L.

that best fit each MIB and geosmin adsorption isotherm of Carbon-A, Carbon-B, and Carbon-C. The SAM successfully described the effect of adsorbent particle size on MIB and geosmin adsorption capacities. Equation 2 of the SMA implies (1) when the adsorbent particle is large enough compared to the penetration depth, the interior region of the adsorbent particle is not used, and adsorption capacity increases with decreasing adsorbent particle size and (2) when the adsorbent particle is small enough compared to the penetration depth, the entire interior region of the adsorbent particle as well as the external region can be utilized for adsorption, and the adsorption capacity is independent of adsorbent particle size. For the case of the MIB adsorption on Carbon-A, the penetration depth ( $1/\alpha$ ) of the SMA was  $\sim 4 \mu\text{m}$  (Table 1). Therefore, the adsorption capacity of increased when the particle diameter was decreased from 31 to 2.6  $\mu\text{m}$ , but it did not change when the particle size was reduced further, to 0.72 or 0.50  $\mu\text{m}$  (Figure 3). For the case of the MIB adsorption on Carbon-B, the penetration depth was  $\sim 30 \mu\text{m}$ , which was larger than the particle diameter of Carbon-B (Table 1). Therefore, the adsorption capacity did not change in the particle size range from 25 to 0.52  $\mu\text{m}$ . The penetration depth differed markedly among carbons, which made adsorption capacity dependency/independency on carbon particle size.

By using eq 3 with the searched parameter values, we next predicted solid-phase concentration profiles across the radius of a carbon particle for deuterium-doped MIB and geosmin adsorbates, in which three hydrogen atoms were replaced with three deuterium atoms (Figure 1). Using the hydrogen content of the carbon particles as determined by the elemental analysis (SI Table S2) and assuming that the earth's natural deuterium/hydrogen molar ratio is 0.00015,<sup>24</sup> we predicted the solid-phase concentration profile of the deuterium/hydrogen ratio along the radius of as-received carbon particles for MIB and geosmin adsorptions (Figure 4). The deuterium/hydrogen atomic ratios decreased from the external surface to the inner region, but for MIB adsorption on Carbon-B and Carbon-C the decrease was less dramatic than for Carbon-A, for which a penetration distance of only  $\sim 4 \mu\text{m}$  was predicted. The deuterium/hydrogen ratio of the outer shell region (to a depth of  $\sim 3 \mu\text{m}$ ) of a Carbon-A (31) particle was predicted to be between 0.004 and 0.013 (Figure 4, left), and these values are  $>30$  times those for the inner region ( $>4 \mu\text{m}$  penetration depth). For the adsorption of geosmin, a higher deuterium/hydrogen ratio was predicted for the outer surface region than for MIB, and the

penetration distances for geosmin were shorter than for MIB for both Carbon-A and Carbon-B (Figure 4, right).

**3.3. Direct Observation of the Solid-Phase Concentration Profile by Means of Isotope Microscopy.** The solid-phase concentration profile was directly observed by using deuterium-doped MIB and Carbon-A (31), which is an adsorbent in which adsorption capacity is particle size-dependent. Prior to visualizing the solid-phase concentration profile, we confirmed that deuterium-doped MIB had the same adsorbability as the nondoped MIB used in the isotherm experiments (Figure 5).

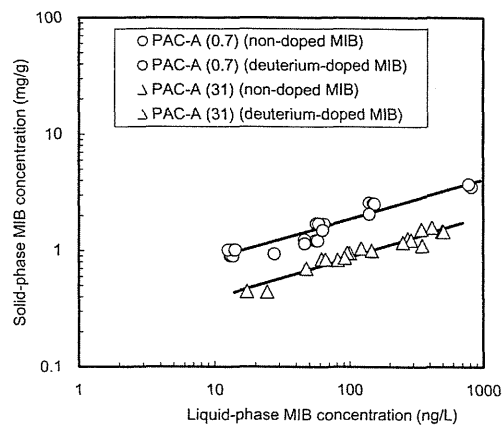
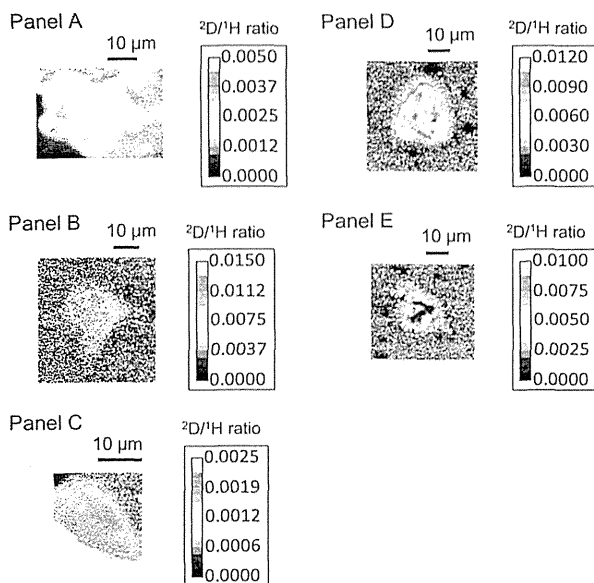


Figure 5. Adsorption isotherms of deuterium-doped 2-methylisoborneol (MIB) and nondoped MIB. PAC, conventionally sized powdered activated carbon.

A series of secondary  $^2\text{D}$  and  $^1\text{H}$  images of a Carbon-A (31) particle loaded with deuterium-doped MIB was taken (SI Figure S4A). Isotopographs were obtained by calculating the ratio of  $^2\text{D}$  detection ( $^2\text{D}_2$  in SI Figure S4A) to  $^1\text{H}$  detection (average of  $^1\text{H}_1$  and  $^1\text{H}_2$  in SI Figure S4A) for each pixel of the image, as shown in Figure 6A. The  $^2\text{D}/^1\text{H}$  ratio was higher than that of the earth's natural  $^2\text{D}/^1\text{H}$  molar ratio of 0.00015, indicating the presence of deuterium-doped MIB that was loaded on the carbon particle. The  $^2\text{D}/^1\text{H}$  ratios across the particle qualitatively confirm greater loading of MIB (higher  $^2\text{D}/^1\text{H}$  ratio) on the exterior region close to the outer-surface of the particle. The trend was confirmed by measurements of another Carbon-A (31) particle also loaded with deuterium-



**Figure 6.** Isotopic maps (deuterium/hydrogen ratio) of carbon particles loaded with deuterium-doped 2-methylisoborneol (MIB) or geosmin. Panel A: coconut-based Carbon-A (31) loaded with deuterium-doped MIB. Panel B: wood-based Carbon-B (25) loaded with deuterium-doped MIB. Panel C: wood-based Carbon-C (19) loaded with deuterium-doped MIB. Panel D: coconut-based Carbon-A (31) loaded with deuterium-doped geosmin. Panel E: wood-based Carbon-B (25) loaded with deuterium-doped geosmin. White dotted lines indicate periphery estimated from the  $^1\text{H}$  images.

doped MIB (SI Figure S5A). The shell adsorption model predicted a  $^2\text{D}/^1\text{H}$  ratio at the exterior region of 0.004 to 0.013; observed ratio was somewhat lower at around 0.004 but roughly agreed with the prediction. The center region exhibits  $^2\text{D}/^1\text{H}$  ratios that are  $\sim 2$ – $3$  times lower than those in the exterior region. It should be noted that the center region of the image (Figure 6A) does not correspond to a radial position of  $r = 0$  as only a portion of the PAC particle was ablated by ion sputtering as shown in Figure 2.

We next examined Carbon-B (25) and Carbon-C (19), which are adsorbents in which adsorption capacity is particle size-independent. For these carbons, we expected MIB to be adsorbed on internal pore surfaces as well as in the external region. For Carbon-B (25), the  $^2\text{D}/^1\text{H}$  ratios were locally high in the internal region, but overall uniform across the particle (Figure 6B, a series of secondary  $^2\text{D}$  and  $^1\text{H}$  images are shown in SI Figure S4B), thereby verifying that MIB adsorbs on interior pore surfaces of Carbon-B (25). For Carbon-C (19), detections were repeated 10 times and during detection a reduction in particle size was clearly observed (SI Figure S4C). We attribute this reduction in size to ablation by ion-beam sputtering, which removed some parts of the particle, in particular the upper part, resulting in a gradual reduction in particle size. Uniform  $^2\text{D}/^1\text{H}$  ratios across the particle were observed, in particular after the third  $^2\text{D}$  detection, suggesting that the inside of the particle was exposed by the ion beam sputtering after the third  $^2\text{D}$  detection. Furthermore, the observed  $^2\text{D}/^1\text{H}$  ratios of Carbon-B (25) and Carbon-C (19) (Figure 6B, C) were consistent with the  $^2\text{D}/^1\text{H}$  ratio predicted by the shell adsorption model (Figure 4, left). These

observations confirm that MIB adsorbs internally on Carbon-B (25) and Carbon-C (19).

We similarly examined the adsorption of deuterium-doped geosmin on Carbon-A (31) and Carbon-B (25). According to the shell adsorption model analysis, geosmin molecules were predicted to adsorb mainly on the exterior region of particles of Carbon-A (31) and Carbon-B (25); therefore, a high  $^2\text{D}/^1\text{H}$  ratio at the exterior region was expected (Figure 4, right). A greater loading of geosmin (high  $^2\text{D}/^1\text{H}$  ratio) near the outer surface of the particles was clearly observed for both Carbon-A (31) and Carbon-B (25) (Figure 6D, E; a series of  $^2\text{D}$  and  $^1\text{H}$  images are shown in SI Figure 3D, E). Clearer pictures were recorded for the geosmin experiments compared with the MIB experiments, which could possibly be due to the greater loading of geosmin compared with that of MIB (see Figure 3).

In this research, isotopic maps of the deuterium/hydrogen ratio, which was a marker of the solid-phase concentration of deuterium-doped MIB and geosmin molecules, provided the direct evidence of the location of adsorbed MIB and geosmin molecules on activated carbon particles. In PAC that had smaller equilibrium adsorption capacity than SPAC, MIB and geosmin principally adsorbed in the exterior shell region of the PAC particles. In contrast, in PAC that had a similar equilibrium adsorption capacity to SPAC, MIB adsorbed more evenly throughout entire PAC particles. Together these results confirm the validity of the shell adsorption theory in which molecules do not completely penetrate the adsorbent particle but instead preferentially adsorb near the outer surface of the particle. The observed equilibrium higher adsorption capacity on SPAC than on PAC was therefore due to the larger external surface area on which the molecules preferentially adsorb.

However, all experiments were conducted in NOM-free waters, but not in natural waters where NOM competition is a significant factor on adsorption.<sup>25</sup> Traditionally, competition is discussed in terms of pore blockage and direct site competition where NOM and micropollutant adsorb in the same pore.<sup>26,27</sup> Our research revealed that micropollutants may adsorb in the external region of carbon particles, that is, in the same region in which chromophoric NOM preferentially adsorbs. Therefore, our results imply that competition is severer when both NOM and micropollutant adsorb in the external region.

## ■ ASSOCIATED CONTENT

### 📄 Supporting Information

Tables S1 and S2 and Figures S1 to S4 are available. This material is available free of charge via the Internet at <http://pubs.acs.org>.

## ■ AUTHOR INFORMATION

### Corresponding Author

\*Phone/fax: +81-11-706-7280; e-mail: [matsui@eng.hokudai.ac.jp](mailto:matsui@eng.hokudai.ac.jp).

### Notes

The authors declare no competing financial interest.

## ■ ACKNOWLEDGMENTS

This study was supported by grants-in-aid for Scientific Research S (24226012) and Challenging Exploratory Research (25550049) from the Japan Society for the Promotion of Science and by a Health and Labour Sciences Research Grant (Research on Health Security Control).

## REFERENCES

- (1) Chowdhury, Z. K.; Summers, R. S.; Westerhoff, G. P.; Leto, B. J.; Nowack, K. O.; Corwin, C. J. *Activated Carbon: Solutions for Improving Water Quality*; American Water Works Association: Denver, CO, 2012.
- (2) Srinivasan, R.; Sorial, G. A. Treatment of taste and odor causing compounds 2-methyl isoborneol and geosmin in drinking water: A critical review. *J. Environ. Sci.* **2011**, *23* (1), 1–13.
- (3) Ando, N.; Matsui, Y.; Kurotobi, R.; Nakano, Y.; Matsushita, T.; Ohno, K. Comparison of natural organic matter adsorption capacities of super-powdered activated carbon and powdered activated Carbon. *Water Res.* **2010**, *44* (14), 4127–4136.
- (4) Ellerie, J. R.; Apul, O. G.; Karanfil, T.; Ladner, D. A. Comparing graphene, carbon nanotubes, and superfine powdered activated carbon as adsorptive coating materials for microfiltration membranes. *J. Hazard. Mater.* **2013**, *261* (0), 91–98.
- (5) Cai, Z.; Wee, C.; Benjamin, M. M. Fouling mechanisms in low-pressure membrane filtration in the presence of an adsorbent cake layer. *J. Membr. Sci.* **2013**, *433* (0), 32–38.
- (6) Huang, H.; Schwab, K.; Jacangelo, J. G. Pretreatment for low pressure membranes in water treatment: A review. *Environ. Sci. Technol.* **2009**, *43* (9), 3011–3019.
- (7) Heijman, S. G. J.; Hamad, J. Z.; Kennedy, M. D.; Schippers, J.; Amy, G. Submicron powdered activated carbon used as a pre-coat in ceramic micro-filtration. *Desalin. Water Treat.* **2009**, *9* (1–3), 86–91.
- (8) Dunn, S. E.; Knappe, D. R. U. *DBP Precursor and Micropollutant Removal by Powdered Activated Carbon*; Water Research Foundation: Denver, CO, 2013.
- (9) Sontheimer, H.; Crittenden, J. C.; Summers, R. S. *Activated Carbon for Water Treatment*. DVGW-Forschungsstelle, Engler-Bunte-Institut; Universität Karlsruhe (TH), 1988.
- (10) Matsui, Y.; Ando, N.; Yoshida, T.; Kurotobi, R.; Matsushita, T.; Ohno, K. Modeling high adsorption capacity and kinetics of organic macromolecules on super-powdered activated carbon. *Water Res.* **2011**, *45* (4), 1720–1728.
- (11) Ando, N.; Matsui, Y.; Matsushita, T.; Ohno, K. Direct observation of solid-phase adsorbate concentration profile in powdered activated carbon particle to elucidate mechanism of high adsorption capacity on super-powdered activated carbon. *Water Res.* **2011**, *45* (2), 761–767.
- (12) Zimin, D.; Craig, V. S. J.; Kunz, W. Adsorption and desorption of polymer/surfactant mixtures at solid–liquid interfaces: Substitution experiments. *Langmuir* **2004**, *20* (19), 8114–8123.
- (13) Zimin, D.; Craig, V. S. J.; Kunz, W. Adsorption pattern of mixtures of trimethylammonium-modified hydroxyethylcellulose and sodium dodecyl sulfate at solid–liquid interfaces. *Langmuir* **2004**, *20* (6), 2282–2291.
- (14) Trabelsi, S.; Langevin, D. Co-adsorption of carboxymethylcellulose and cationic surfactants at the air–water interface. *Langmuir* **2006**, *23* (3), 1248–1252.
- (15) Hoffmann, I.; Opper, C.; Gernert, U.; Barreleiro, P.; von Rybinski, W.; Grdzielski, M. Adsorption isotherms of cellulose-based polymers onto cotton fibers determined by means of a direct method of fluorescence spectroscopy. *Langmuir* **2012**, *28* (20), 7695–7703.
- (16) Hoffmann, I.; Theile, M.; Grätz, S.; Scholz, J.; Barreleiro, P.; von Rybinski, W.; Grdzielski, M. On the influence of surfactants on the adsorption of polysaccharide-based polymers on cotton studied by means of fluorescence spectroscopy. *Langmuir* **2012**, *28* (31), 11400–11409.
- (17) Ahn, S.; Werner, D.; Karapanagioti, H. K.; McGlothlin, D. R.; Zare, R. N.; Luthy, R. G. Phenanthrene and pyrene sorption and intraparticle diffusion in polyoxymethylene, coke, and activated carbon. *Environ. Sci. Technol.* **2005**, *39* (17), 6516–6526.
- (18) Sakamoto, N.; Seto, Y.; Itoh, S.; Kuramoto, K.; Fujino, K.; Nagashima, K.; Krot, A. N.; Yurimoto, H. Remnants of the early solar system water enriched in heavy oxygen isotopes. *Science* **2007**, *317* (5835), 231–233.
- (19) Yurimoto, H.; Nagashima, K.; Kunihiro, T. High precision isotope micro-imaging of materials. *Appl. Surf. Sci.* **2003**, *203–204* (0), 793–797.
- (20) Benninghoven, A.; Rüdenauer, F. G.; Werner, H. W. *Secondary Ion Mass Spectrometry: Basic Concepts, Instrumental Aspects, Applications and Trends*; Wiley: New York, 1987.
- (21) Kita, N. T.; Ushikubo, T.; Fu, B.; Valley, J. W. High precision SIMS oxygen isotope analysis and the effect of sample topography. *Chem. Geol.* **2009**, *264* (1–4), 43–57.
- (22) Hamasaki, T.; Matsumoto, T.; Sakamoto, N.; Shimahara, A.; Kato, S.; Yoshitake, A.; Utsunomiya, A.; Yurimoto, H.; Gabazza, E. C.; Ohgi, T. Synthesis of <sup>18</sup>O-labeled RNA for application to kinetic studies and imaging. *Nucleic Acids Res.* **2013**, DOI: 10.1093/nar/gkt344.
- (23) Matsui, Y.; Yoshida, T.; Nakao, S.; Knappe, D. R. U.; Matsushita, T. Characteristics of competitive adsorption between 2-methylisoborneol and natural organic matter on superfine and conventionally sized powdered activated carbons. *Water Res.* **2012**, *46* (15), 4741–4749.
- (24) Drever, J. I. *The Geochemistry of Natural Waters: Surface and Groundwater Environments*; Prentice Hall PTR, 1997.
- (25) Chen, G.; Dussert, B. W.; Suffet, I. H. Evaluation of granular activated carbons for removal of methylisoborneol to below odor threshold concentration in drinking water. *Water Res.* **1997**, *31* (5), 1155–1163.
- (26) Guo, Y.; Yadav, A.; Karanfil, T. Approaches to mitigate the impact of dissolved organic matter on the adsorption of synthetic organic contaminants by porous carbonaceous sorbents. *Environ. Sci. Technol.* **2007**, *41* (22), 7888–7894.
- (27) Summers, R. S.; Knappe, D. R. U.; Snoeyink, V. L. Adsorption of organic compounds by activated carbon. In *Water Quality and Treatment: A Handbook of Community Water Supplies*; Edzwald, J. K.; American Water Works Association, McGraw-Hill, 2011; Chapter 14.

